Turbulence-induced secondary motion in a buoyancy-driven flow in a circular pipe

Yannick Hallez and Jacques Magnaudet
INPT, UPS, IMFT (Institut de Mécanique des Fluides de Toulouse), Université de Toulouse, Allée Camille Soula, F-31400 Toulouse, France and CNRS, IMFT, F-31400 Toulouse, France

(Received 13 June 2009; accepted 17 July 2009; published online 25 August 2009)

We analyze the results of a direct numerical simulation of the turbulent buoyancy-driven flow that sets in after two miscible fluids of slightly different densities have been initially superimposed in an unstable configuration in an inclined circular pipe closed at both ends. In the central region located midway between the end walls, where the flow is fully developed, the resulting mean flow is found to exhibit nonzero secondary velocity components in the tube cross section. We present a detailed analysis of the generation mechanism of this secondary flow which turns out to be due to the combined effect of the lateral wall and the shear-induced anisotropy between the transverse components of the turbulent velocity fluctuations. © ***2009 American Institute of Physics***.
[DOI: 10.1063/1.3213246]

Since Prandtl's group pioneering investigations,[1] high-Reynolds-number incompressible flows in curved channels or in straight noncircular ducts are known to involve secondary mean motions. Centrifugal or other nonconservative body forces perpendicular to the main motion tend to skew the primary spanwise vorticity in developing flows, leading to transverse motions whose magnitude can be up to 20%–30% of the streamwise velocity. Secondary flows typically one order of magnitude smaller are also known to exist in fully-developed turbulent flows in straight rectangular ducts.[2] These weak secondary motions, known as Prandtl's secondary flows of second kind, are due to the inhomogeneity of the transverse Reynolds stresses near the corners of the duct and result in a pair of counter-rotating streamwise vortices near each corner. They have been the subject of several detailed investigations, as they induce significant transport of momentum and heat within the duct cross section and also because their prediction represents a serious challenge for one-point turbulence models.[3] During a joint experimental/numerical investigation of buoyancy-induced turbulent mixing in an inclined tube (see Refs. 4 and 5 for more detail on the experiments), we observed the existence of a secondary mean motion whose topology and sustaining mechanism differ from those of the secondary flows reported so far, since it arises in a straight circular pipe in presence of a fully-developed primary flow. It is the purpose of this letter to describe the structure of this, apparently undocumented, secondary flow and elucidate its generating mechanism.

The physical configuration we consider is as follows. A circular pipe of diameter $\boldsymbol{d}$ and length $\boldsymbol{L}$ closed at both ends ($\boldsymbol{x}=\pm\boldsymbol{L}/2$) is filled with two miscible (i.e., with zero interfacial tension) low-viscosity fluids of different densities ($\rho_2>\rho_1$) in such a way that each fluid initially occupies half of the pipe length, the two fluids being separated by a lock at $\boldsymbol{x}=0$. The pipe is tilted at an angle Θ from the vertical in such a way that the arrangement is unstable, owing to buoyancy. After the lock is removed at time $\boldsymbol{t}=0$, the light (heavy) fluid tends to flow along the upper (lower) part of the cross section toward the upper (lower) end wall, forming a stably stratified turbulent countercurrent flow where turbulent mixing takes place. As far as the fronts of both currents remain far from the end walls, this relative motion results in a turbulent shear flow which, in the region $|\boldsymbol{x}|\ll\boldsymbol{L}/2$ on which we focus in this letter, is statistically independent of both $\boldsymbol{x}$ and $\boldsymbol{t}$.

The results to be discussed below were obtained by solving the three-dimensional, time-dependent Navier–Stokes equations for a variable-density incompressible flow (with no explicit reference to the Boussinesq approximation), together with the density equation, assuming molecular diffusivity to be negligibly small. The computations were carried out in a $176\boldsymbol{d}$ long circular pipe of diameter $\boldsymbol{d}$, using a cylindrical grid with $32\times64\times2816$ grid points in the radial, azimuthal, and streamwise directions, respectively. Details regarding the computational technique and the validation of the code may be found elsewhere[6] and are not repeated here. In the example discussed below, we select a tilt angle $\Theta=15°$, an Atwood number $\mathrm{At}=(\rho_2-\rho_1)/(\rho_2+\rho_1)=10^{-2}$ and a Reynolds number $\mathrm{Re}=\boldsymbol{V_t d}/\nu=790$ with $\boldsymbol{V_t}=(\mathrm{At}\,\boldsymbol{gd})^{1/2}$, $\boldsymbol{g}$ denoting gravity and ν being the kinematic viscosity which we assume to be identical in both fluids. The $(\boldsymbol{x},\boldsymbol{t})$ averaging procedure was performed throughout a $9\boldsymbol{d}$-long window centered at $\boldsymbol{x}=0$, starting at time $\boldsymbol{T_I}(\mathrm{At}\,\boldsymbol{g}/\boldsymbol{d})^{1/2}=177$ and continued until the final time of the computation, $\boldsymbol{T_F}(\mathrm{At}\,\boldsymbol{g}/\boldsymbol{d})^{1/2}=554$, so that the averaged quantities (hereinafter denoted with angle brackets) result from averaging over 180 000 time steps and 384 grid cells.

Let the $\boldsymbol{x}$-axis be along the streamwise ascending direction, the $\boldsymbol{z}$-axis be such that the $(\boldsymbol{x},\boldsymbol{z})$ plane is vertical with $\boldsymbol{z}>0$ in the ascending direction, and the $\boldsymbol{y}$-axis be horizontal and such that the Cartesian $(\boldsymbol{x},\boldsymbol{y},\boldsymbol{z})$ coordinate system is right-handed with $\boldsymbol{y}=\boldsymbol{z}=0$ on the tube centerline. The averaged velocities in the vertical diametrical plane $\boldsymbol{y}=0$ are shown in Fig. 1. The streamwise velocity $\langle\boldsymbol{U}\rangle$ exhibits the expected $\boldsymbol{S}$-shape with an almost constant shear except in the

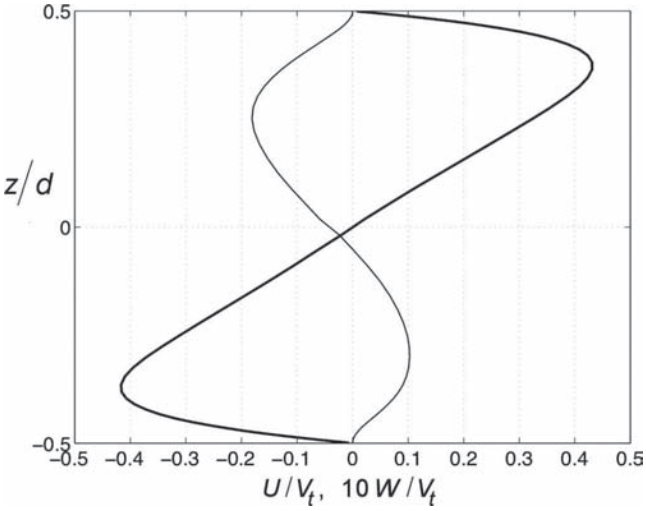

FIG. 1. Averaged velocity profiles in the vertical midplane. Bold line: streamwise velocity; thin line: crosswise velocity. Lengths are normalized by the pipe diameter $\boldsymbol{d}$ and velocities are normalized by $\boldsymbol{V_t}=(\mathrm{At}\,\boldsymbol{gd})^{1/2}$.

vicinity of the wall. The puzzling feature of the flow is the crosswise velocity $\langle \boldsymbol{W}\rangle$ which is seen to be nonzero even though it is typically only 3%–5% of $\langle \boldsymbol{U}\rangle$. This secondary velocity is negative (positive) in the upper (lower) part of the vertical midplane, indicating that the fluid converges toward the center of the pipe for $\boldsymbol{y}\approx 0$. The complete spatial structure of the secondary velocity field is shown in Fig. 2, together with the so-called swirling strength λ_{ci} which is commonly used as a criterion allowing the identification of vortical structures in three-dimensional flows (λ_{ci} is defined as the imaginary part of the conjugate eigenvalues of the velocity gradient tensor[7]). This plot confirms the presence of four stationary streamwise vortices within the pipe cross section. Note that the secondary flow revealed by Fig. 2 only

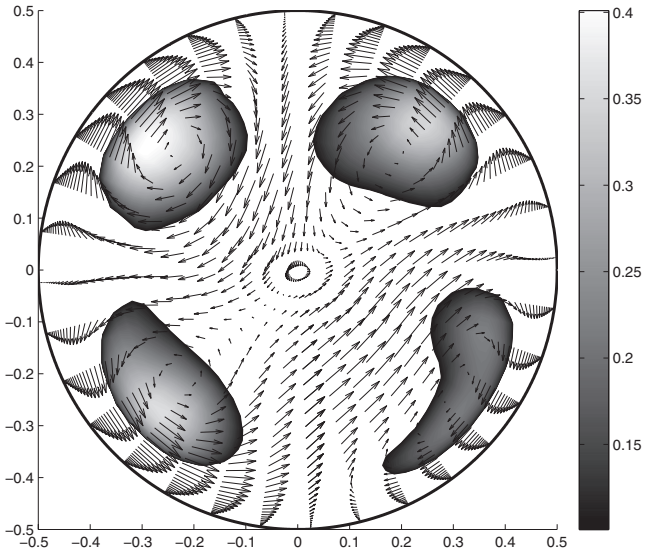

FIG. 2. Mean secondary flow and streamwise vortices identified by the magnitude of the swirling strength (λ_{ci} criterion). The normalization is similar to that of Fig. 1.

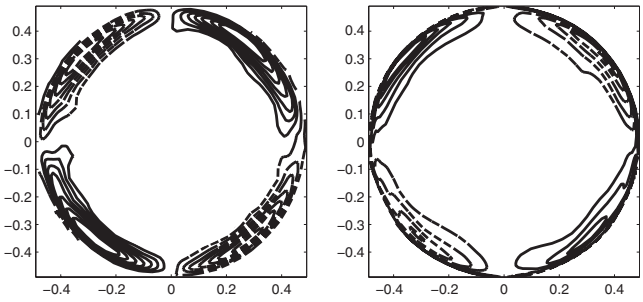

FIG. 3. Map of the turbulent term $\mathcal{R}$ (left) and baroclinic term $\mathcal{B}$ (right) in Eq. (1), both normalized by $(\boldsymbol{V_t}/\boldsymbol{d})^2$. The contour levels of $\mathcal{R}$ range from -0.342 to 0.342 with a step of 0.049, while those of $\mathcal{B}$ range from -0.085 to 0.085 with a step of 0.015. Solid (dashed) lines denote positive (negative) values. The zero level has been removed for clarity.

exhibits approximate left-right and top-bottom symmetries, owing to the limited sampling time allowed by the computational run.

Obviously the nonzero secondary mean flow is directly related to the existence of a nonzero mean component of the streamwise vorticity Ω (we omit the brackets for simplicity) whose magnitude (not shown here) is observed to be $\boldsymbol{O}[(\mathrm{At}\,\boldsymbol{g}/\boldsymbol{d})^{1/2}]$, even though the mean secondary velocities themselves are only a few percents of the primary velocity $\langle \boldsymbol{U}\rangle$. We shall come back to this point later.

To elucidate the origin of the secondary mean flow, we need to consider the balance equation for Ω. Since the mean flow is both stationary and homogeneous in the streamwise direction, this equation reduces to

$$\langle \boldsymbol{V}\rangle \partial_{\boldsymbol{y}}\Omega + \langle \boldsymbol{W}\rangle \partial_{\boldsymbol{z}}\Omega = \mathcal{B} + \mathcal{R} + \nu(\partial^2_{\boldsymbol{yy}} + \partial^2_{\boldsymbol{zz}})\Omega, \tag{1}$$

where

$$\mathcal{B} = \langle (\partial_{\boldsymbol{y}}\rho\partial_{\boldsymbol{z}}\boldsymbol{p} - \partial_{\boldsymbol{z}}\rho\partial_{\boldsymbol{y}}\boldsymbol{p})/\rho^2\rangle,$$
$$\mathcal{R} = \partial^2_{\boldsymbol{yz}}(\langle v'^2\rangle - \langle \boldsymbol{w}'^2\rangle) - (\partial^2_{\boldsymbol{yy}} - \partial^2_{\boldsymbol{zz}})\langle v'\boldsymbol{w}'\rangle, \tag{2}$$

$\boldsymbol{p}$, ρ, v', and $\boldsymbol{w}'$ standing for the pressure, density, and turbulent velocity fluctuations along the $\boldsymbol{y}$- and $\boldsymbol{z}$-axes, respectively. The first and last terms in Eq. (1) represent the transport of Ω by the mean secondary flow and its diffusion by viscous effects, respectively, so that both of them remain zero if the mean flow is parallel. Therefore the generation of Ω is due to term $\mathcal{B}$ resulting from baroclinic effects and to term $\mathcal{R}$ induced by variations of the secondary Reynolds stresses within the cross section.

The numerical data were used to evaluate the latter two terms throughout the pipe cross section. Figure 3 indicates that both terms are concentrated near the wall and exhibit a four-lobe structure which is antisymmetric with respect to the horizontal and vertical axes. The baroclinic torque $\mathcal{B}$ is typically five times smaller than the turbulent term $\mathcal{R}$. Hence, while buoyancy effects drive the main flow, they are not at the root of the secondary flow. The turbulent term $\mathcal{R}$ appears to be the key of the generation of the streamwise vorticity, suggesting that the present secondary flow is of Prandtl's second type. To elucidate the origin of the secondary flow, it is thus necessary to understand the spatial struc-

ture of the secondary Reynolds stresses. The spatial distribution of $\mathcal{R}$ and $\mathcal{B}$ revealed by Fig. 3 clearly suggests that the lateral wall plays a key role in the mechanism, even though no geometrical anisotropy exists here, in contrast with the case of a rectangular duct. The other crucial ingredient, which is specific to the present situation, is the existence of the nonaxisymmetric mean shear $\partial_z\langle \boldsymbol{U}\rangle$ in the flow. This salient characteristic of the primary flow, which results directly from the existence of the light ascending and heavy descending currents, does not exist in a usual Poiseuille flow, allowing $\langle \boldsymbol{U}\rangle$ to be almost constant in the core in the latter case. Several classical studies of the turbulent structure in homogeneous shear flows have revealed that, in presence of a constant and nonzero $\partial_z\langle \boldsymbol{U}\rangle$, the three main Reynolds stresses are such that $\langle \boldsymbol{u}'^2\rangle > \langle v'^2\rangle > \langle \boldsymbol{w}'^2\rangle$.[8–10] This is because the turbulent fluctuation, which is produced only along the $\boldsymbol{x}$-direction, is then unevenly redistributed along the other two directions, owing to the anisotropic transport and stretching induced by the shear. In particular Refs. 9 and 10 found the ratio $\langle v'^2\rangle^{1/2}/\langle \boldsymbol{w}'^2\rangle^{1/2}$ to range from 1.15 to 1.5, depending on the time ratio $\boldsymbol{S}^*=\boldsymbol{T_t}\partial_z\langle \boldsymbol{U}\rangle$, $\boldsymbol{T_t}$ denoting the large-eddy turnover time. In presence of a stable stratification characterized by the Richardson number $\mathrm{Ri}=(\boldsymbol{g}\langle\partial_z\rho\rangle/\rho)(\partial_z\langle \boldsymbol{U}\rangle)^{-2}$, $\langle v'^2\rangle^{1/2}/\langle \boldsymbol{w}'^2\rangle^{1/2}$ has been found to increase from about 1.28 for $\mathrm{Ri}=0$ to about 1.44 for $\mathrm{Ri}=1$, which reflects the gradual inhibition of vertical motions as Ri increases.[11] Present results indicate $\langle v'^2\rangle^{1/2}/\langle \boldsymbol{w}'^2\rangle^{1/2}=1.3$ with $\mathrm{Ri}=0.07$ near the diametrical midplane $\boldsymbol{z}=0$, Ri being based on the effective gravity $\boldsymbol{g}\sin\Theta$ in the $\boldsymbol{z}$-direction. Hence the anisotropy level determined in the present computations is consistent with known results and indicates that the main cause of the difference in magnitude between the spanwise fluctuation v' and the crosswise fluctuation $\boldsymbol{w}'$ in the core of the flow is the shear rather than the stratification.

Within a large part of the pipe cross section, the mean shear is almost constant (see Fig. 1) so that the flow is close to a homogeneous turbulent shear flow. Hence the anisotropy level determined above does not vary much and the cross-correlation $\langle v'\boldsymbol{w}'\rangle$ is also almost zero since the $\boldsymbol{y}$-axis is a principal axis of the time-averaged flow. This allows us to conclude that the whole term $\mathcal{R}$ is negligibly small outside the peripheral region directly influenced by the wall. Since the main gradients lie along the radial direction in the near-wall region, the analysis of this region is more easily achieved in cylindrical coordinates. Defining the polar coordinate system $(\boldsymbol{r},\theta)$ so that $(\boldsymbol{r},\theta,\boldsymbol{x})$ is right-handed and introducing the associated radial and azimuthal velocity fluctuations $(v_{\boldsymbol{r}},v_\theta)$, it may be shown that the generation term becomes $\mathcal{R}=(1/\boldsymbol{r}^2)\partial^2_{\boldsymbol{r}\theta}[\boldsymbol{r}(\langle v_{\boldsymbol{r}}^2\rangle-\langle v_\theta^2\rangle)]-[\partial^2_{\boldsymbol{rr}}-(1/\boldsymbol{r}^2)\partial^2_{\theta\theta}+(3/\boldsymbol{r})\partial_{\boldsymbol{r}}]\langle v_{\boldsymbol{r}}v_\theta\rangle$. In a constant-density turbulent flow in a circular pipe, no average quantity depends on θ and $v_{\boldsymbol{r}}$ and v_θ are uncorrelated, so that the above expression of $\mathcal{R}$ makes it clear that no secondary flow can exist in this case. Considering that the thickness $\delta(\theta)$ of the near-wall boundary layer is much less than the pipe radius implies that, in the vicinity of the wall, the radial derivative of any Reynolds stress involved in $\mathcal{R}$ is proportional to $1/\delta(\theta)$ and thus dominates over terms with a $1/\boldsymbol{r}$ prefactor. Hence, although the relative magnitude of $\langle v_{\boldsymbol{r}}v_\theta\rangle$ and $\langle v_{\boldsymbol{r}}^2\rangle-\langle v_\theta^2\rangle$ is unknown, one has at leading order in both contributions $\mathcal{R}\approx(1/\boldsymbol{r})\partial^2_{\boldsymbol{r}\theta}(\langle v_{\boldsymbol{r}}^2\rangle-\langle v_\theta^2\rangle)-\partial^2_{\boldsymbol{rr}}\langle v_{\boldsymbol{r}}v_\theta\rangle$.

Within the viscous sublayer adjacent to the wall (which given the modest Reynolds number extends approximatively up to $\boldsymbol{r}/\boldsymbol{d}=0.4$ here), v_θ ($v_{\boldsymbol{r}}$) varies linearly (quadratically) with the distance $\boldsymbol{d}/2-\boldsymbol{r}$, owing to the no-slip condition and the divergence-free constraint. Therefore we may write $\langle v_{\boldsymbol{r}}^2\rangle-\langle v_\theta^2\rangle\approx-\alpha(\theta)(\boldsymbol{d}/2-\boldsymbol{r})^2$, with $\alpha(\theta)>0$, by which we conclude that the radial derivative $\partial_{\boldsymbol{r}}(\langle v_{\boldsymbol{r}}^2\rangle-\langle v_\theta^2\rangle)$ is positive close to the wall, whatever the azimuthal location θ. Since the mean velocity $\langle \boldsymbol{U}\rangle$ reaches its maximum at some radial location $\boldsymbol{r}=\boldsymbol{r_M}(\theta)$ and returns to zero for $\boldsymbol{r}=\boldsymbol{d}/2$, a negative mean shear exists in the range $\boldsymbol{r_M}(\theta)<\boldsymbol{r}<\boldsymbol{d}/2$. This negative shear is maximum in the vertical midplane (see Fig. 1) and is zero in the diametrical midplane $\boldsymbol{z}=0$ where the mean velocity is almost zero whatever the spanwise location. Hence, owing to the generic shear-induced anisotropy of the Reynolds stresses discussed above, we expect $\langle v_\theta^2\rangle$ to be larger near the top and bottom of the cross section, where it corresponds to the spanwise fluctuation, than near the midplane $\boldsymbol{z}=0$ where it corresponds to the crosswise fluctuation. This behavior, which is confirmed by Fig. 4 (left), implies $\partial_\theta\alpha>0$ (<0) in the first and third (second and fourth) quadrants, so that the same conclusion holds for the whole term $(1/\boldsymbol{r})\partial^2_{\boldsymbol{r}\theta}(\langle v_{\boldsymbol{r}}^2\rangle-\langle v_\theta^2\rangle)$.

Let us now consider the contribution to $\mathcal{R}$ of the cross-correlation $\langle v_{\boldsymbol{r}}v_\theta\rangle$ which, according to the near-wall behavior of $v_{\boldsymbol{r}}$ and v_θ, evolves like $\beta(\theta)(\boldsymbol{d}/2-\boldsymbol{r})^3$ within the viscous sublayer. To determine the sign of β, it is useful to note the geometrical property $\langle v_{\boldsymbol{r}}v_\theta\rangle=-\frac{1}{2}(\langle v'^2\rangle-\langle \boldsymbol{w}'^2\rangle)\sin 2\theta+\langle v'\boldsymbol{w}'\rangle\cos 2\theta$. We may then take advantage of the left-right and top-bottom symmetries of all second-order moments (keeping in mind that in a homogeneous turbulent shear flow with a mean shear $\partial_z\langle \boldsymbol{U}\rangle$ the $\boldsymbol{y}$-axis is a principal direction) to conclude that $\langle v_{\boldsymbol{r}}v_\theta\rangle$ is zero for both $\boldsymbol{y}=0$ and $\boldsymbol{z}=0$. Hence we expect $\langle v_{\boldsymbol{r}}v_\theta\rangle$ to reach its maximum strength along the two diagonals $\theta=\pm\pi/4$, where $\langle v_{\boldsymbol{r}}v_\theta\rangle=\mp(\langle v'^2\rangle-\langle \boldsymbol{w}'^2\rangle)/2$. These various conclusions are confirmed by Fig. 4 (right). As we saw above, the mean shear results in a positive difference $\langle v'^2\rangle-\langle \boldsymbol{w}'^2\rangle$ throughout the core of the pipe, so that β is negative (positive) along the first (second) diagonal. As the sign of the second derivative $\partial_{\boldsymbol{rr}}\langle v_{\boldsymbol{r}}v_\theta\rangle$ follows that of β, we conclude that the contribution $-\partial_{\boldsymbol{rr}}\langle v_{\boldsymbol{r}}v_\theta\rangle$ to $\mathcal{R}$ is positive (negative) within the first and third (second and fourth) quadrants.

Coming back to Eq. (1) it turns out that, whatever their relative magnitude, both leading terms in $\mathcal{R}$ have the same four-lobe structure and the same sign in each quadrant, i.e., $\mathcal{R}$ is >0 (<0) within the first and third (second and fourth) quadrants, in agreement with the results displayed in Fig. 3 (left).

The final point to be addressed is that of the scaling of the secondary flow obtained through the above mechanism. The first estimate we need is that of $\mathcal{R}$. In the present flow, the wall shear stress is responsible for the turbulent velocity fluctuations in the region where $\mathcal{R}$ is nonzero. The mean axial velocity goes from zero at the wall to its maximum

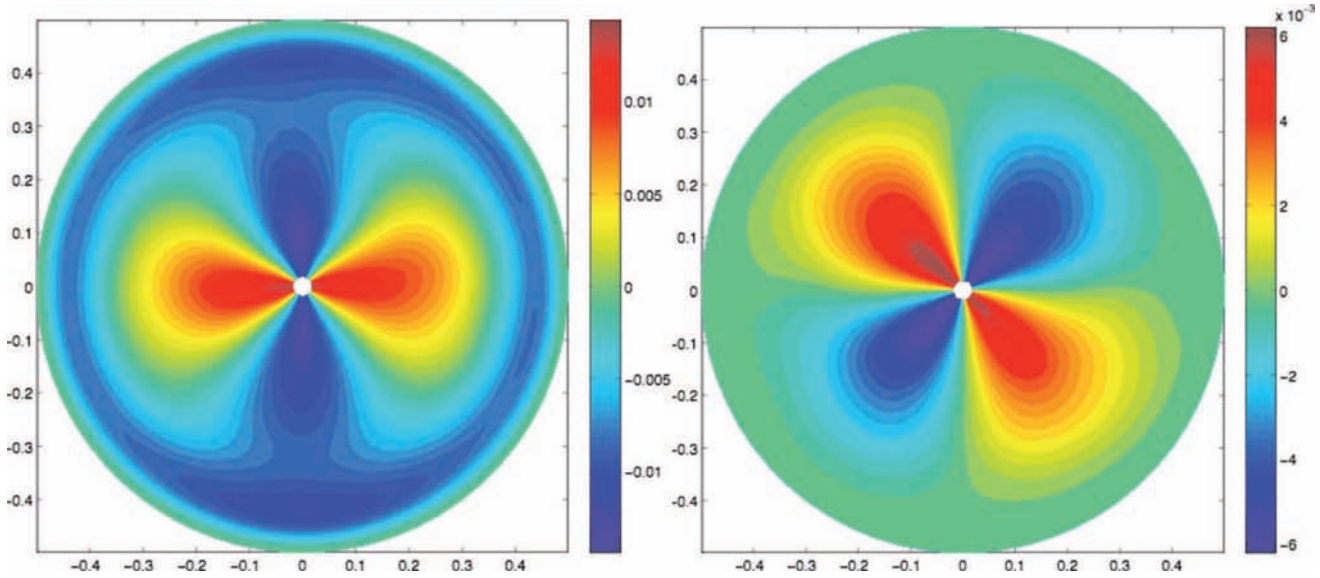

FIG. 4. (Color online) Map of the secondary anisotropy $\langle v_r^2\rangle - \langle v_\theta^2\rangle$ (left) and cross correlation $\langle v_r v_\theta\rangle$ (right), both normalized by $\boldsymbol{V_t^2}$.

$\boldsymbol{O}(\boldsymbol{V_t})$ value within the boundary layer of thickness $\delta = \boldsymbol{O}(\mathrm{Re}^{-1/2}\boldsymbol{d})$, so that the wall shear stress scales like $\boldsymbol{O}(\mathrm{Re}^{1/2}\rho\nu\boldsymbol{V_t}/\boldsymbol{d})$. Thus the magnitude u of the velocity fluctuations obeys $\rho u^2 = \mathrm{Re}^{1/2}\rho\nu\boldsymbol{V_t}/\boldsymbol{d}$, implying $u^2/\boldsymbol{V_t^2} = \mathrm{Re}^{-1/2}$ [note, however, that within the viscous sublayer $\langle v_r v_\theta\rangle$ is smaller than $\langle v_\theta^2\rangle$ by $\boldsymbol{O}(\mathrm{Re}^{-1/2})$, owing to its cubic variation with the distance to the wall as compared to the quadratic variation of $\langle v_\theta^2\rangle$]. It is then straightforward to determine the magnitude of $\mathcal{R}$ by noting that the radial variation of the turbulent stresses arises within the viscous sublayer of thickness $\boldsymbol{O}(\delta)$, whereas their azimuthal variation arises over one-fourth of the pipe perimeter, i.e., over an $\boldsymbol{O}(\boldsymbol{d})$ distance. Obviously this azimuthal variation (and the correlation between v_r and v_θ) also depends on the dimensionless shear rate $\boldsymbol{S}^*$ through some function $\boldsymbol{F}(\boldsymbol{S}^*)$ that vanishes for $\boldsymbol{S}^* = 0$. Here the turnover time of the large-scale turbulent motions is governed by the mean shear, so that $\boldsymbol{S}^* = \boldsymbol{O}(1)$. The aforementioned results on homogeneous sheared turbulence[9–11] indicate that the Reynolds stress anisotropy does not vary much with $\boldsymbol{S}^*$ in this range, so that here $\boldsymbol{F}$ may simply be regarded as a nonzero constant. All this implies that $\mathcal{R}$ is of $\boldsymbol{O}[(\boldsymbol{V_t}/\boldsymbol{d})^2]$, as indicated by Fig. 3 (left). Very close to the wall, $\mathcal{R}$ is balanced by the viscous diffusion of the streamwise vorticity [last term in Eq. (1)]. This diffusion arises within the boundary layer, so that the diffusion term is of $\boldsymbol{O}(\nu\Omega/\delta^2)$, which implies $\Omega = \boldsymbol{O}(\boldsymbol{V_t}/\boldsymbol{d})$. Finally, the secondary velocities reach their typical magnitude $\boldsymbol{V_S}$ near $\boldsymbol{r} = \boldsymbol{d}/2 - \delta$, so that the transport term in Eq. (1) is of $\boldsymbol{O}[\boldsymbol{V_S}\boldsymbol{V_t}/(\delta\boldsymbol{d})]$ and this term balances $\mathcal{R}$ at this radial location, thus implying $\boldsymbol{V_S} = \boldsymbol{O}(\boldsymbol{V_t}\delta/\boldsymbol{d}) = \boldsymbol{O}(\mathrm{Re}^{-1/2}\boldsymbol{V_t})$. These conclusions are consistent with the features displayed by the computational results. In particular we recover the already noticed feature that Ω is of the order of $\boldsymbol{V_t}/\boldsymbol{d}$, even though the mean secondary velocities are only a few percents of $\boldsymbol{V_t}$ (here $\mathrm{Re} = 790$, so that $\mathrm{Re}^{-1/2} \approx 0.036$).

The above qualitative analysis allows the spatial structure and sign of the source term $\mathcal{R}$ in Eq. (1) and the scaling of the resulting streamwise vorticity and secondary velocities to be correctly predicted. This supports the idea that the secondary flow observed in our computations and recently confirmed in experiments[5] is a special case of Prandtl's secondary flow of second kind which results from the combined effect of the mean shear and the lateral wall on the turbulence structure.

This research has been funded by the ANR through Grant No. ANR-07-BLAN-0181. We are grateful to F. Moisy for stimulating discussions on the generation mechanism of the secondary flow.

[1] L. Prandtl, "Über die ausgebildete turbulenz," Verfahren diese Zweite Internationale Kongress für Technische Mechanik, Zürich (1926) ["Turbulent flow," NACA Technical Memo 435 (1927), p. 62].
[2] P. Bradshaw, "Turbulent secondary flows," Annu. Rev. Fluid Mech. **19**, 53 (1987).
[3] A. O. Demuren and W. Rodi, "Calculation of turbulence-driven secondary motion in non-circular ducts," J. Fluid Mech. **140**, 189 (1984).
[4] T. Séon, J. P. Hulin, D. Salin, B. Perrin, and E. J. Hinch, "Buoyant mixing of miscible fluids in tilted tubes," Phys. Fluids **16**, L103 (2004).
[5] J. Znaien, "Étude locale du mélange de deux fluides dans la géométrie confinée d'un tube incliné," Ph.D. thesis, Université Paris 11, 2009.
[6] Y. Hallez and J. Magnaudet, "Effects of channel geometry on buoyancy-driven mixing," Phys. Fluids **20**, 053306 (2008).
[7] J. Zhou, S. Balachandar, and T. M. Kendall, "Mechanisms for generating coherent packets of hairpin vortices in channel flow," J. Fluid Mech. **387**, 353 (1999).
[8] V. G. Harris, J. A. H. Graham, and S. Corrsin, "Further experiments in nearly homogeneous turbulent shear flow," J. Fluid Mech. **81**, 657 (1977).
[9] S. Tavoularis and S. Corrsin, "Experiments in nearly homogenous turbulent shear flow with a uniform mean temperature gradient. Part 1," J. Fluid Mech. **104**, 311 (1981).
[10] S. Tavoularis and U. Karnik, "Further experiments on the evolution of turbulent stresses and scales in uniformly sheared turbulence," J. Fluid Mech. **204**, 457 (1989).
[11] H.-J. Kaltenbach, T. Gerz, and U. Schumann, "Large-eddy simulation of homogeneous turbulence and diffusion in stably stratified shear flow," J. Fluid Mech. **280**, 1 (1994).